Powder Technology 419 (2023) 118346

Contents lists available at ScienceDirect

Powder Technology

journal homepage: www.journals.elsevier.com/powder-technology

Experimental metrics of the powder layer quality in the selective laser sintering process

Marco Lupo [1], Sina Zinatlou Ajabshir, Daniele Sofia, Diego Barletta, Massimo Poletto [*]

Dipartimento di Ingegneria Industriale, Università degli Studi di Salerno, via Giovanni Paolo II, 132, 84084 Fisciano, SA, Italy

HIGHLIGHTS

- A dedicated experimental set-up was built to mimic the SLS spreading step.
- A layer surface analysis starting from microphotographs is proposed.
- A wavelet analysis of grey-level profiles was carried out.
- A metric of the powder layer quality based on indicators derived from the wavelet analysis was developed.
- The proposed metric on powder spreadability provides consistent results that cannot be inferred from powder flowability.

GRAPHICAL ABSTRACT

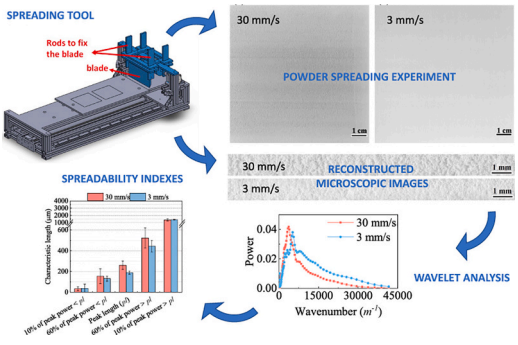

ARTICLE INFO

Keywords:
Powder layer
Selective laser sintering
Spreading
Image analysis

ABSTRACT

According to the literature, the microscopic quality of the powder layer produced in the Selective Laser Sintering (SLS) process is related to the onset of macroscopic defects of the produced powder. This study proposes an experimental procedure able to quantify the quality of the powder layer obtained in the spreading step of the SLS process. A dedicated experimental set-up was developed, able to mimic the powder spreading step of the SLS process and to allow the photographic analysis of its surface. Four commercial polymeric powders for SLS applications were tested at two different speeds of the recoater. An image processing analysis was developed, converting a series of microscopic images of layer surface in grey level profiles along the spreading direction. The grey level profiles were further analysed with a wavelet analysis tool, and the major features of the wavelet powder spectral density were used to calculate specific indicators of the powder layer quality. The different indicators provide consistent results comparing the tested powders and the testing conditions. The powder ranking according to spreadability indexes differs from the one obtained using flowability indexes. This finding confirms that spreadability cannot be directly related to flowability.

* Corresponding author.
E-mail address: mpoletto@unisa.it (M. Poletto).
[1] Presently at Granutool, Rue Jean Lambert Defrêne 107, 4340 Awans, Belgium.

https://doi.org/10.1016/j.powtec.2023.118346
Received 7 December 2022; Received in revised form 12 February 2023; Accepted 14 February 2023
Available online 19 February 2023

1. Introduction

Interest in powder-based additive manufacturing (AM) has been growing fast for several industrial sectors of application [1] producing artefacts made of several materials such as metals, ceramics, polymers, and composites [2]. These techniques allow significant waste minimisation for the possibility of reprocessing powder excesses and make this production method more sustainable and cheaper than the traditional ones [3] [4]. In Selective Laser Sintering (SLS), objects are produced by the alternating spreading of powder layers and aimed sintering of parts of these layers with the use of a laser source with automated procedures that allow building the geometrical features reported in a CAD drawing [5]. SLS can be relatively inexpensive if compared with other manufacturing processes. However, its main disadvantages are related to the long-time requirements for the process [2], especially for large-size objects, poor surface finishing [6] and low mechanical resistance [2]. In particular, these drawbacks can be due to the non-uniform morphology of the powder bed formed during the spreading step [7]. For this reason, in the last years, a large number of studies focused on the relevance of this part of the process.

1.1. Powder flowability in the spreading process

Prescott and Barnum [8] defined powder *flowability* as the propensity to flow in a specific process unit. Therefore, the same powder can behave differently in different process conditions. In SLS, flowability plays a key role because it directly affects the quality of the sintered components. Good spreading conditions are necessary for tighter powder packing, more homogeneous powder layers and smoother layer surfaces, leading to better mechanical and surface properties of the final object [9]. On the contrary, higher porosity or large roughness of the layer could lead to weaker bonds between sintered layers and, consequently, poor mechanical resistance of the artefact [9]. Therefore, it is important to understand whether a powder is suitable to be used in the SLS process by evaluating its capacity to be spread on a plate and underlying powder layers, commonly named spreadability [10]. It is important to highlight that, even if they are related, flowability and spreadability should not be intended as synonyms [11].

Several methods to evaluate the flowability of powders have been reported in the literature. However, their relevance to SLS depends on the ability of the flowability characterisation to reproduce the proper consolidation conditions of the spreading process. Powder spreading is a dynamic process in which different powder mechanisms occur, as highlighted by Chen et al. [12] or Yao et al. [13]. Fig. 1 represents a schematic view of the main steps that a powder parcel encounters in the spreading process: 1) powder avalanching on the front surface of the heap moving in front of the blade; 2) powder deposition at the base of the moving front; 3) powder shear in front of the blade inside the moving heap; 4) a fast stress transition in the forming layer between finite shear stress in front of the blade and zero shear stress in the back. The different flow properties testing methods found in the literature may be relevant to one or more of the above-enumerated steps.

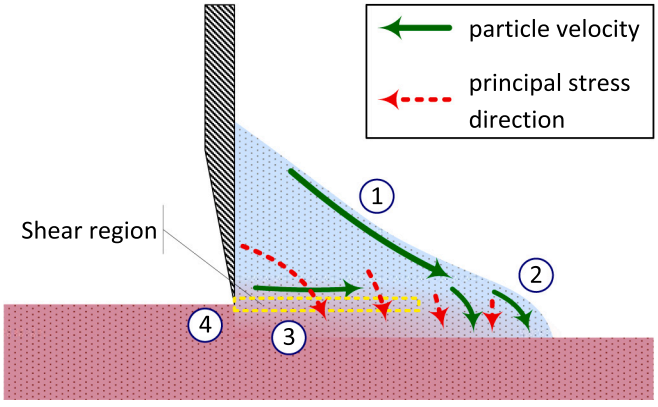

Fig. 1. Main flow steps in the powder spreading process: 1) avalanching on the leading side of the moving heap; 2) deposition at the heap front; 3) internal shear in front of the blade; 4) stress release on the formed layer.

Schmid et al. [14] proposed to use the Hausner ratio, HR, (i.e. the ratio between tap and bulk density) measured by a simplified and rigorous procedure and by round-robin tests of different laboratories to minimise the uncertainty of results. The simplified procedure seems relevant to step 2, represented in Fig. 1. In fact, according to the authors, it resulted adequate to characterise and rank different SLS powders. However, it can be argued that HR might not be appropriate to evaluate the powder flowability in SLS, where powder layers form under very low consolidation conditions and without vibrations.

Defined consolidation methods like shear testers have been used to characterise the flow properties of SLS polymeric powders at ambient and high temperatures up to the melting point [15,16] utilising the High Temperature-Annular Shear Cell (HT-ASC) [17]. In these studies, cohesive and frictional properties were characterised at lower consolidation ranges (up to 1 kPa), even though this condition might not be the same during the layer formation [18]. In fact, the layer quality produced by step 4, represented in Fig. 1, is likely to be strongly correlated to the powder cohesion determined by the dynamic consolidation process occurring in step 3 in front of the blade. Ruggi et al. [16] found that the granular Bond (Bo) number was a relevant indicator of the critical powder flowability for effective spreading in SLS machines. Temperature effect was also observed in terms of a poorer flowability for different polyamide powders when approaching the respective melting temperature.

Dynamic methods have also been used to characterise powders for SLS. Fereiduni et al. [19] claimed that the interaction between the twisted blade impeller and the powder in a Freeman FT4 Powder Rheometer might resemble that of the spreading blade with the powder appearing as step 3 in Fig. 1. In fact, the torque for the rotation of a twisted blade impeller in a fixed bed of particles is measured at low consolidation conditions, even if non-quantitatively specified. The latter measures the resistance to flow of powders when close to a non-consolidated or stress-free condition. Hence it is an indirect measurement of the powder flowability. Several characterisation studies reported the specific energy to compare the flowability of different powders for SLS [20–22].

Rotating drums have also been used to investigate the dynamic flow of SLS powders during spreading [18,23–25]. The conditions reported may be similar to step 1 in Fig. 1. However, with this setup, some properties directly related to powder cohesion were also evaluated. Amado and his co-workers [23,24] derived from rotating drum experiments (Revolution Powder Analyzer, Mercury Scientific Inc.) different physical parameters: the avalanche angle, the surface fractal and the volume expansion ratio (VER). The first one corresponds to the angle that the powder surface contour forms with a horizontal line in correspondence with the maximum potential energy before the fall of the powder. The surface fractal, which corresponds to the fractal dimension of the free surface of the powder, is an indicator of the rugosity of the powder surface. A low surface fractal means low rugosity and, therefore, a good distribution of the powder. VER is the ratio between the volume occupied by the powder in the drum and the volume obtained after a consolidation procedure by tapping. Therefore, optimal SLS powders should have low avalanche angle, surface fractal and VER. However, by analysing the results, the authors observed that sometimes variations of VER and surface fractal with the material were not consistent. For example, the tested thermoplastic elastomer showed a higher surface fractal than a polyamide-based material but lower VER. Therefore, Amado et al. [23] combined VER and the surface fractal in one parameter to consider both the effects of the Rank Index, which is the ratio between VER and the surface fractal: the higher the index, the

better the powder flowability. A similar setup, the GranuDrum rotating drum (Granutools, B) [25], was used to evaluate the powder flowability through the flowing angle (i.e. the dynamic angle of repose) of Ti alloys, at different rotating speeds corresponding to different applied shear rates, as an indicator of the uniformity of powder layers in Selective Laser Melting [26]. Later, Amado et al. [24] modified the aluminium rotating drum with a heated core cylinder to heat the powder to 293 K to explore typical temperatures of the conventional SLS process, up to values just below the melting point of the material [27]. Above the glass transition temperature of a commercial polyamide 12, better flowability was observed due to a more homogenous packing of the bed of particles.

All the methods mentioned above try to assess whether a powder has sufficient flowability for the SLS process or not. However, all of them are indirect and do not necessarily provide exhaustive information on powder spreadability. In fact, during the spreading process, powders likely experience a state of stress that can be different from that occurring during the tests with indirect instruments such as a rotating drum or a shear cell. As a result, direct methods can be preferred to verify the spreadability of powders in conditions as similar as possible to those occurring during the spreading with a tool such as a blade or a roller. Some examples of direct methods are reported in the following section.

1.2. Methods of analysis of the quality of the powder layer

Several recent works have focused on the experimental assessment of the quality of spread powder layers [7,10,28–31]. In these experiments, powders were subjected to the process represented in Fig. 1, including all the steps. A first qualitative visual analysis of the surface quality and the study of the layer density was proposed by Van den Eynde et al. [28].

Ahmed et al. [29] manually produced a powder layer with a blade and then “froze” it with an adhesive spray. The quality of the layer surface was analysed using an image analysis tool on SEM images by detecting empty patches as proof of transient jamming [32] of the powder in the heap forming in front of the moving blade and flowing through the gap between the blade and the previous layer. More recently, a step forward was put using a shadowgraphy technique to highlight the surface roughness and the linear defects along the spreading direction [30]. A promising algorithm based on single-particle detection was recently proposed by Mitterlehner et al. [31].

Snow et al. [10] claimed that the spreadability of metal powders was indicated by the fraction of the area of the building plate covered by powder, the rate of powder deposition, and the rate of change of the avalanche angle. These parameters could be somehow correlated with the angle of repose of the powder. A similar concept was recently followed in numerous experimental works, in which it was argued that the spreadability was proportional to the mass of particles within the spread layer [33] or to the packing density in the layer [34,35].

A deeper insight into the powder layer structure was provided by in situ x-ray imaging techniques [7,36]. Escano et al. [7] focused on particle-scale dynamics to derive the repose angle, the slope surface speed, the slope surface roughness and the dynamics of powder clusters at the powder front as indicators of powder flow behaviour during spreading. Oropeza et al. [36], reporting spatially resolved powder layer density measurements in a spreading testbed, did not limit to providing average density values but obtained the cumulative distributions, which appear to be a more informative indicator of the uniformity of the particle distribution across the spread layer.

A comprehensive comparison between conventional powder flowability testing methods and a spreading test was carried out by Mehrabi et al. [37] on two SLS metal powders. They introduced spreadability, defined as the ratio between the spread layer's average density and the powder's bulk density. In particular, the average density of the spread layer was calculated as the ratio of the mass of powder collected in a pocket 1 mm deep engraved on the plate in which the powder spreading experiment was carried out and the pocket volume. The bulk density is intended as the density of the powder in the feeding bed of the SLS apparatus. Such value is well defined in the case of free-flowing powders as the metal powders tested in the study.

Sofia [38] developed a simple blade-spreading tool for powder on a plate and a procedure to estimate the layer surface roughness by analysing images of a laser blade hitting the layer surface. He found a correlation between surface roughness and the condition approaching the onset of macroscopic irregularity of the layer. This result indicates the study of the surface quality of the powder layer as a tool to classify the results of powder spreading experiments quantitatively.

The literature indicated that measuring the layer porosity is a reliable tool for evaluating the quality of the layer spread. However, the powder porosity is often indirectly measured from layer density evaluations that require a destructive procedure for the generated layer. Shadowgraph analysis, mentioned above, is a relatively cheap and promising procedure. However, it requires the definition of the appropriate metrics to relate the image features with the powder spreadability and possibly understanding differences between powders close to conditions at which macroscopic defects are produced. In order to carry out a reliable powder spreading process to study the quality of the produced layer, a new experimental setup was developed at the University of Salerno. It allows the reproduction of different spreading conditions, such as the shape of the spreading tool, the spreading speed and the gap height below the tool. In this work, this experimental setup was used to test several polymeric powders at different scrolling velocities of the blade used as a spreading tool.

Furthermore, a new image analysis procedure, based on the derivation of the wavelet power spectrum, is proposed to assess the surface quality of experimental powder layers quantitatively. This procedure is based on the study of the characteristic lengths of the shadow profiles. It has the advantage of scarcely depending on the powder colour, the image brightness and contrast, and, to a certain extent, the quality of the image used for the analysis. The quantitative results are compared with those of a standard shear testing procedure, with the idea in mind that possibly the shear testing may provide relevant values of powder cohesion that may be responsible for the quality of the powder layer determined by step 4 in Fig. 1, as mentioned above.

2. Experimental apparatuses, procedures and materials

2.1. Powder spreading

2.1.1. Apparatus

An experimental setup was developed to reproduce the powder spreading process occurring in a typical SLS machine. The main parts of the setup were the spreading system, composed of a blade and a roller recoater, and a deposition plate (Fig. 2). The blade could be inclined with respect to the vertical position, and experiments can be carried out at different angles of the blade. Different scrolling velocities of the blade could also be adopted. Moreover, the roller recoater could be used as an alternative to the blade at different scrolling and rotational velocities. In principle, the equipment might also be equipped with different diameter rollers.

Three different deposition plates could be used. Each presents two square trays of 10 cm side, each with a fixed depth of 100, 200 and 300 μm. The aim was to create powder layers with the same thickness as the depth of the trays. The depths of the tray adopted were within the range of layer thicknesses used in the SLS process [39]. The first of the two trays was used to load the powder with a procedure that leaves an excess of powder over the plate level to mimic the powder loading procedure in SLS machines, including the powder lifting process in the powder loading compartment. Therefore, this tray was called “collection tray” (CT). The recoater pushed the powder from the CT towards the “deposition tray” (DT), the second of the two trays of the deposition plate. In particular, as explained in more detail in the following, it was possible to adjust the quantity of powder over the DT. In general, the amount adopted was the one that ensured that the powder spread with the

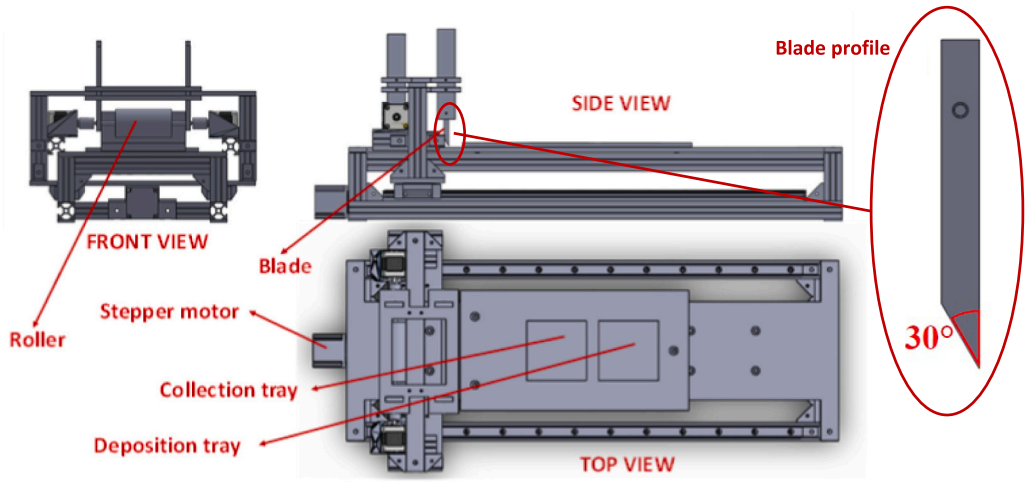

Fig. 2. Different views of the setup used for powder spreading.

recoater was sufficient to fill the DT, including the powder dispersion associated with the recoating process. The precision of the manufacturing of the DT is critical for the significance of the experiments, and the tolerances adopted in the manufacturing process were very low and tailored to the minimum depth of the tray, i.e. 100 μm. The spreading plate was 10 mm thick. Such a value ensured a large plate stiffness and that any non-uniformity or unevenness of the powder layer could be attributable only to the quality of the powder spreadability and the other parameters of the spreading process and not o defects of the depth of the deposition tray.

The results presented in this work refer only to the blade used as recoater and to the deposition plate of 300 μm depth. Keeping the same layer thickness for different materials is consistent with the practice frequently adopted in commercial SLS apparatuses, even if it may not always seem reasonable when using powders with different particle size distributions. The thickness chosen, however, is much larger than d_{90} for all the powder tested reported in Section 2.1.3 below. Therefore, according to the studies by Ghadiri's research group at the University of Leeds [32,40], the systems tested should be far from the jamming phenomena and be suitable to study the effect on the layer quality due to powder cohesion.

It is known from the literature also that roller recoaters or fixed recoaters with shapes different from the blade may provide a better layer surface [41,42]. However, their use introduces other parameters to the spreading process that requires an optimisation process that may depend on the properties of the material used. To keep a more straightforward comparison between the powder spreading experiment and powder flowability, one of the primary objectives of this work, the blade was adopted, leaving the optimisation of the spreading process as further work to be done.

To analyse the powder layer all over its surface, a system for the image analysis of the layer surface through a microscope was mounted on the same bridge used to move the spreading apparatus. It consisted of a microscope equipped with a digital mechanically connected to the bridge. In particular, two long screws allowed the microscope to be moved in both the vertical direction (z) and the perpendicular direction (y) with respect to the spreading direction (x). Moreover, the microscope could be rotated around the y-axis (Fig. 3a) according to the θ_M angle. By using the recoater advancement set up (Fig. 3a), it was possible to move the microscope in the x-direction along the position defined by their movement in the y-direction. The microscope's focus was adjusted by moving the camera in the z-direction. The camera used with the microscope to take photos of the powder layer (Fig. 3a) was an AmScope MU1603 16 MP, connected to a computer via USB 3.0. A led lamp with a 30 W LED with an inclination of 45° (Fig. 3b) with respect to the layer

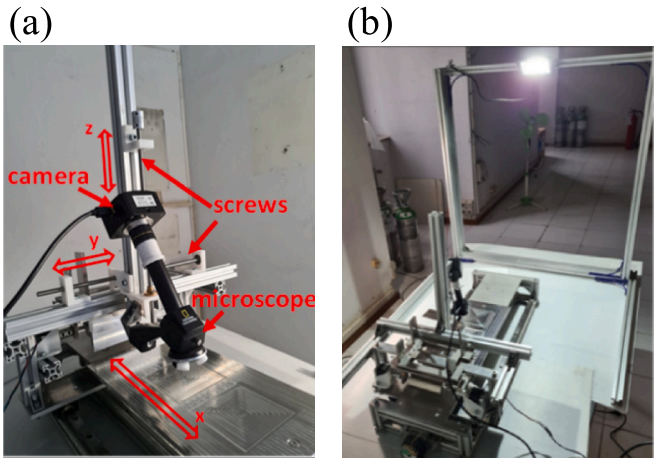

Fig. 3. (a) Movements of the microscope and the camera in x, y and z-direction; (b) adequate lighting implemented on the powder beds for the image analysis.

was used to illuminate the layer surface.

2.1.2. Procedures

Before starting the experiments, to avoid the effect of moisture condensed from air humidity, powders were dried at 100 °C for 1 h and sieved using a mesh of 250 μm size to retain clusters with dimensions larger than the maximum particle diameter. Without a heating system on the setup for the experiments presented, all the measurements were carried out after cooling down the powder at ambient temperature at which all measurements were carried out. The procedure does not avoid the presence of capillary condensation but at least minimises its effects. Test repetitions indicated acceptable repeatability of the experimental procedure. The drying temperature of 100 °C is at least 20 °C below the lowest melting temperature (Table 1) of the polymers used, ensuring sufficient particle stability according to Ruggi et al.'s findings [16].

The procedure adopted in the tests aimed at reproducing as closely as possible the spreading process conditions in a double bed SLS machine in which the feeding bed is raised above the level of the blade edge, and the powder sintering bed is lowered of a quantity equal to the thickness of a layer. In an SLS machine, this allows that, with a single movement, the blade recoater takes the material from the feeding bed and generates the new powder layer of the desired thickness by moving forward towards the sintering bed. Therefore, in this work, the bed preparation procedure included two parts. The first was, dedicated to generating the

Table 1
Material properties of PA6 powder: T_m is the melting temperature; ρ_B is the bulk density of the powder; ρ_P is the density of the solid; d_{10}, d_{50} and d_{90} are the particle diameters corresponding to the 10th, 50th and 90th percentile of the cumulative particle size, respectively; $d_{3,2}$ is the Sauter mean diameter, $d_{4,3}$ is the the volume mean diameter.

Materials	T_m (°C)	ρ_B (kg/m^3)	ρ_P (kg/m^3)	d_{10} (μm)	d_{50} (μm)	d_{90} (μm)	$d_{3,2}$ (μm)	$d_{4,3}$ (μm)
PA6	210	525	1130	15	46	91	20	50
PA6 LM black	193	590	1370	40	74	129	66	80
PPNAT	140	330	890	35	69	122	36	74
TPU	120–150	500	1100	28	82	163	35	90

powder layer higher than the surface of the plate over the collection tray, simulating the raised feeding bed. The second part was dedicated to the powder transfer from the collection tray to the deposition tray, simulating the generation of a new layer over the sintering bed. The details of how this was achieved are reported in Supplementary Material I.

The powder layer was photographed by coupling the optical microscope with a 10× magnification and the camera. The basic idea was that measuring the asperity size could indicate the width of the surface roughness. The height of the LED lamp in the spreading direction was adjusted to have the light hitting the powder layer surface at about 45° of inclination from the horizontal. With such illumination, layer asperities could be detected because darker regions on the surface images corresponded to the side of the surface asperities illuminated by a more inclined light. At the same time, the height adopted would minimise the projection of shadows from the front asperity on the trailing one. In fact, using more inclined light would artificially increase the layer surface affected by shadows, with the risk that shadows of larger asperities could hide smaller ones, reducing the procedure's detection sensitivity.

Using the supporting system described above, in which the microscope and the camera were connected to the recoater bridge, it was possible to look at the powder layer at different points keeping the same illumination and the same distance between the microscope and particles. The resulting similar powder magnification in the images allowed the direct comparison of images taken at different positions and on different powder layers. Furthermore, by combining images taken at adjacent positions along the direction of motion of the bridge, it was possible to reconstruct images of stripes of the layer taken parallel to the recoater advancement direction and at different lateral positions (in the y direction). The details of this procedure are reported in Supplementary Material I.

The images were analysed in MATLAB by using the "Wavelet Toolbox" [43]. The aim was to derive the time-averaged wavelet power spectrum for each image and, consequently, to infer information regarding the quality of the powder layer. Details of this procedure are given in Supplementary Material I and II.

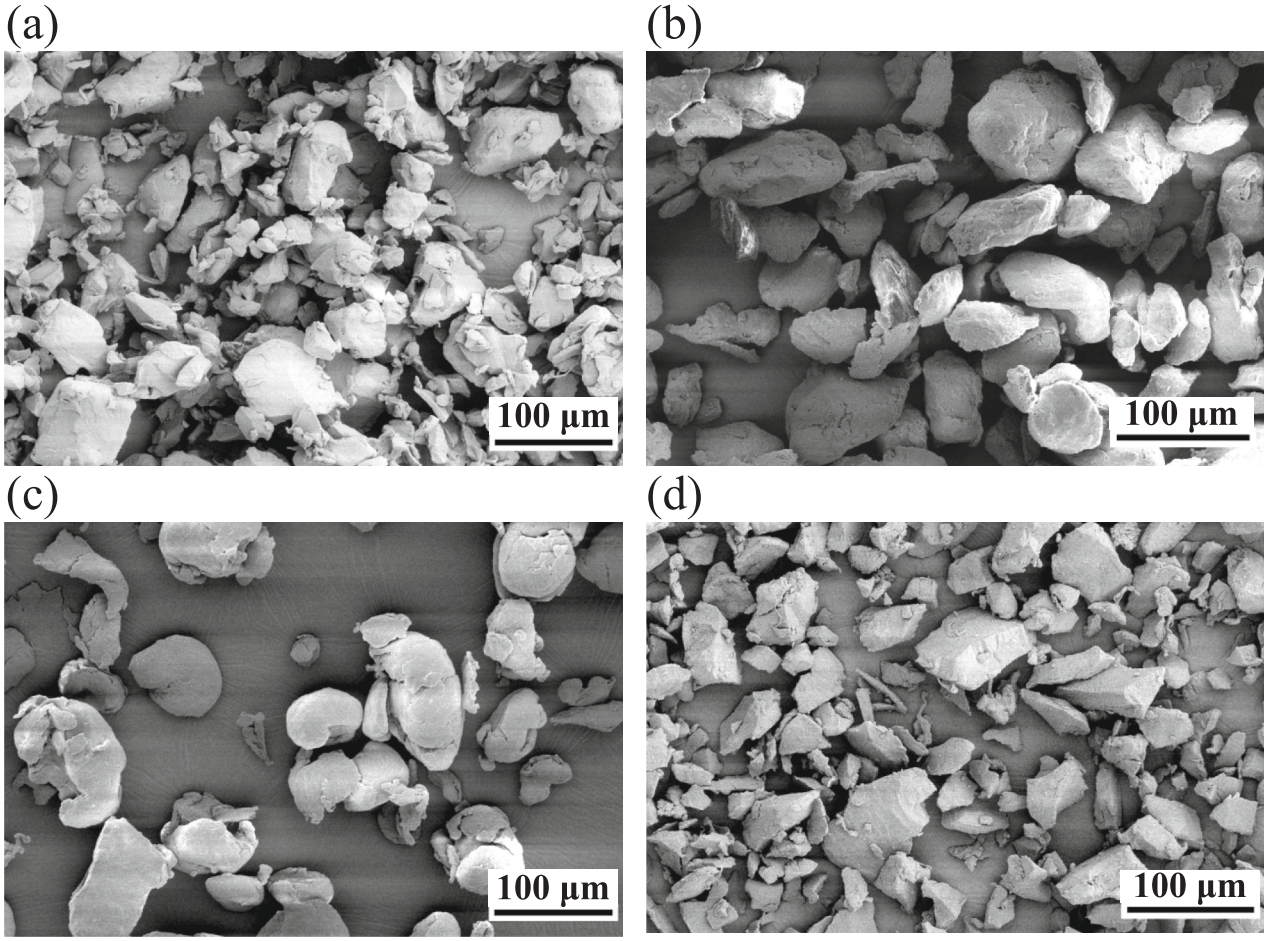

Fig. 4. SEM images: (a) PA6; (b) PA6Black; (c) PPNAT and (d) TPU.

2.1.3. Materials

The five polymeric powders studied in these experiments were chosen between purposely designed for the SLS process. The material properties derived from the technical data sheet and direct characterisation are reported in Table 1.

Moreover, to compare the effect of the particle shape and morphology, microscopy analysing was done by Scanning Electron Microscopy. Fig. 4 illustrates SEM images, all taken at 500× magnification.

2.2. Shear test

The powder flowability was measured with an Anton Paar Shear cell mounted on the Modular Compact Rheometer MCR 302 WESP. After filling the bottom ring of the cell with the powder and levelling the powder surface, a complete flow function was evaluated by measuring four different yield loci at 1, 2, 4 and 8 kPa pre-shear normal stresses and room temperature. All shear test Experiments were repeated 4 times. The values of the pre-shear normal stresses are lower than usual in shear stress experiments since the adopted values were considered more appropriate for the powder spreading process in selective laser sintering. The flow function results for the powder are plotted in Fig. 5, where dashed lines report the constant flow factors ($ff = \sigma_1/f_c$) values separating the classes according to the Jenike classification of flowability. The flow factor of all powders at room temperature is generally in the free-flowing range. At the lowest consolidation stress considered, greater difficulty in measuring the flow behaviour was experienced, but this did not increase the uncertainty of the measurements results. However, it can be concluded that the PA6 powder had the best flowability compared to TPU, PA6 Black, and PPNAT powders.

3. Results and discussion

Experimental tests were carried out at two values of the scrolling or spreading velocity of the blade (V_S), namely 30 mm/sand 3 mm/s. Each test was repeated at least 2 times to verify the reproducibility of the results. For each test, fresh powder (not used before) was used after drying and sieving, as described previously.

The macroscopic and microscopic images of PA6 powder layers are reported in Fig. 6 as an example of the results obtained with all materials. The macroscopic images were obtained by using a 12 MP camera. Visual inspection of macroscopic images reported in Fig. 6 (a) and (b) does not reveal significant differences in layer surface quality for the two spreading velocities. Instead, in microscopic images reported in Fig. 6

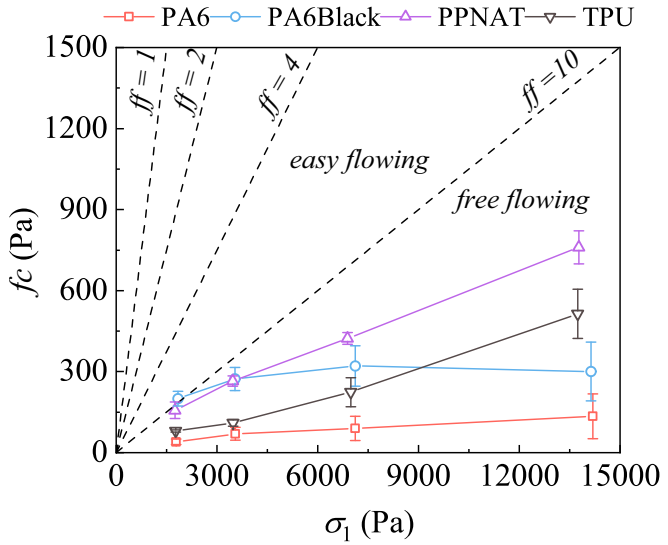

Fig. 5. Material flow functions.

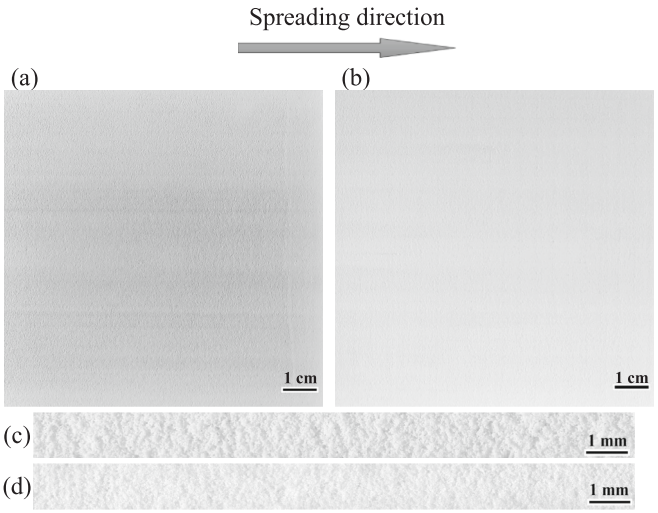

Fig. 6. PA6 powder layer after spreading, macroscopic top view: (a) 30 mm/s; (b) 3 mm/s and microscopic view: (c) 30 mm/s; (d) 3 mm/s.

(c) and (d), some qualitative differences in roughness can be read by inspecting the distribution and the size of brighter and darker areas.

As a result, time-averaged wavelet power spectrum analysis was carried out on microscopic images to obtain more quantitative indications related to surface roughness. Fig. 7 reports the microscopic images extracted from the powder layers spread at both values of the spreading velocity tested and the corresponding time-averaged wavelet power spectra for the four tested materials. In Supplementary Material III, additional images and their corresponding wavelet power spectra are reported. Provided the image reconstruction procedure described in Section 2.1.2, it appears that the images reconstructed in Fig. 7 are characterised by uniform illumination. Generally, this is a good starting point for any image analysis based on light intensity distributions. Of course, all the image exposures were chosen so that the brightness level in the powder image did not reach saturation. It is worth noting that inspection of Fig. 7 reveals that the analysis proposed is scarcely dependent on the average brightness level of the image. In fact, the procedure adopted for determining the layer quality measures characteristic distances between regions of changing grey levels. Therefore, the results are only marginally affected by the light intensity, provided that uniform lighting of the field. This finding appears clearly in Fig. 7, where powders providing images with entirely different average brightness (such as that in Fig. 7b) are characterised by power spectral densities in the same ranges of ordinate values.

The distribution of the lengths characterising for the powder surface roughness were derived from the time-averaged wavelet power spectra. In particular, due to the shape of the power spectrum function, the analysis was not limited to identifying the peak length, *pl*, as the inverse of the wavenumber, corresponding to the maximum value of the power (i.e. the peak value). In particular, it also considered other 4 length values corresponding to power values equal to the 10% and 60% of the peak value taken both in the lower and the upper end (i.e. for lengths smaller or larger than *pl*), as detailed in Supplementary Material I. In this way, it was possible to obtain five characteristic lengths for each powder and each spreading velocity. Results are shown in the histogram plots reported in Fig. 8, where the black bars correspond to the standard deviation of results obtained in different tests.

Inspection of Fig. 8 suggests that the surface roughness characteristic lengths are somehow affected by the scrolling velocity of the blade. In particular, the intermediate lengths characterising the distribution (i.e. *pl* and lengths at 60% of peak power) generally decrease with decreasing blade spreading velocity for PA6 and PA6 black powders. As a result, assuming that lower roughness length values correspond to a more uniformly spread powder surface, a better quality surface layer was

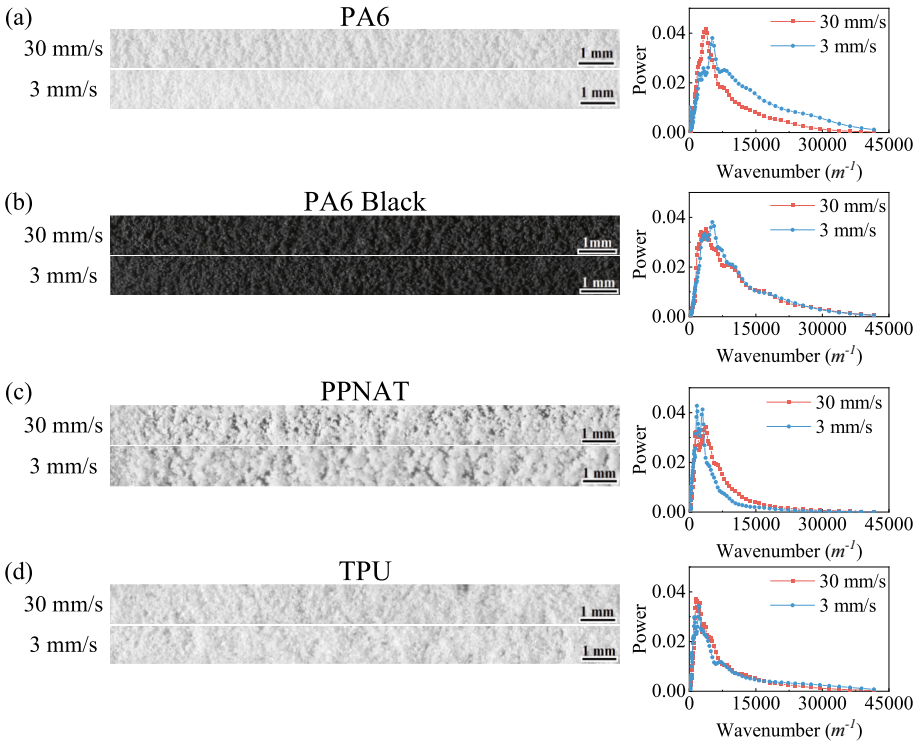

Fig. 7. Images of the powder layers and corresponding time-averaged wavelet power spectra obtained for PA6, PA6 black, PPNAT and TPU at two spreading velocities (30 mm/s and 3 mm/s).

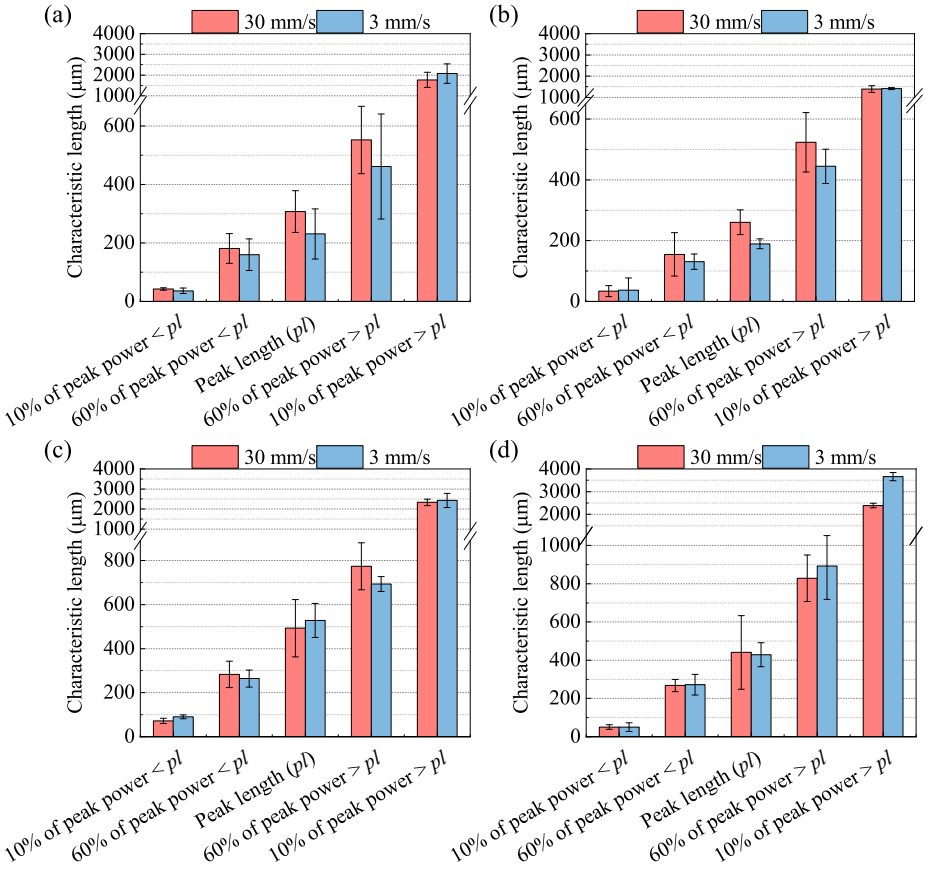

Fig. 8. Values of lengths characterising the distribution of the powder's surface roughness: (a) PA6; (b) PA6Black; (c) PPNAT; (d) TPU.

obtained for these powders at lower blade scrolling velocity. Consistently, a negative effect of the recoater speed on the quality of the layer spread was previously observed on metal powders by Mehrabi et al. [37], operating with a blade and by Chen et al. [34] and Oropeza et al. [36] working with a counterrotating roller. A much more limited effect of the blade velocity was observed for PNAT and TPU powders. It was not possible to identify the common flowability or particle features of these two powders able to suggest the reason for this limited effect.

Comparing the characteristic lengths of the surface layer roughness and accounting for the particle size distribution could help. Therefore, for each powder, Table 2 reports the values of the peak length *pl* divided by the median particle size d_{50} and the ratio between the range of lengths, including spectral values above 60% of the peak value in the distribution, lr_{60}, and *pl*. Assuming that increased values of lr_{60} would correspond to less peaked distribution and indicate better quality ranges, the data of lr_{60}/ppl are consistent with those of pl/d_{50}. In fact, comparing results at different velocities worst values of the uniformity of the powder surface at higher speed for the same powder (so at equal d_{50}) are detectable in terms of both lower values of *pl* and higher value of lr_{60} for PA6, PA6Black and TPU powders. The opposite appears for PPNAT powders.

Ranking the powders according to the quality of the spread powder layer, the so-called "spreadability", in terms of increasing values of pl/d_{50} and decreasing values of lr_{60}/pl, the ordered sequence should be PA6Black > TPU > PA6 > PPNAT. The series slightly changes at 3 mm/s in terms of pl/d_{50}, providing an inversion between TPU and PA6. It should be acknowledged, however, that these two powders report very similar results both in terms of pl/d_{50} and lr_{60}/ppl. Therefore an inversion, in this case, may also depend on experimental uncertainty.

It is remarkable that the just reported "spreadability" ranking just reported does not correspond to the flowability ranking of the powders obtainable by comparing flow factors. Table 2 also reports the values of the material flow factor at the minimum value of the consolidation stress attainable and corresponding to about 1.8 kPa (ff @ σ_{1min}). In fact, the flowability ranking of the tested powder would, in this case, be PA6 > TPU > PPNAT>PA6Black, remarkably, with a complete change of the ranking position of PA6Black. This discrepancy between powder flowability and powder spreadability has also been reported on metal powders by Mehrabi et al. [37].

There are several possible reasons why flowability measured with shear testing may not be fully representative of the spreading process. All the steps of the spreading processes appearing in Fig. 1 are strongly affected by powder cohesion that is quantified by shear testing experiments. Its procedure is conceived in two steps to make shear testing repeatable and relevant to the hopper flow for which it was developed. The first step is meant to attain shear at steady state, a condition that is, in fact, representative of the powder shear inside large pieces of equipment, such as silos or process hoppers, and a second shearing step at which the material resistance to shear is measured [44]. In the powder deposition process, reported as step 2 in Fig. 1, the normal stress applied to the powder is limited by its weight. The subsequent powder strain in the shear zone occurring in front of the bade in step 3 in Fig. 1 may also be limited. Therefore, the combination of these features of steps 2 and 3 may not guarantee the attainment of the steady state in the shear step of the shear testing procedure. Consequently, the strict relationship between the effect of powder cohesion on the quality of the layer formed in step 4 and the cohesion measured in a conventional shear testing experiment may not be justified.

Table 2
Comparison between flowability and characteristic lengths of the roughness of the layer surface.

		PA6	PA6Black	PPNAT	TPU
30 mm/s	ff @ σ_{1min}	44.7	9.2	11.2	22.1
	pl/d_{50}	6.7	3.5	7.1	5.4
	lr_{60}/pl	1.21	1.42	1.00	1.28
3 mm/s	pl/d_{50}	5.0	2.6	7.7	5.2
	lr_{60}/ppl	1.31	1.66	0.81	1.45

4. Conclusions

The developed experimental protocol and image analysis procedure allowed a quantitative assessment of the roughness of the layer surface obtained by spreading four different polymeric powders used in the selective laser sintering process. In particular, length scales representing the predominant values of the roughness lengths and width of their distribution were identified using a wavelet analysis tool. Lower values of the dominant length, and larger values of the prevailing length ranges, have been associated with the quality of the powder layers. If normalised to the particle size, these parameters provide a consistent metric for powder spreadability. Accordingly, it was possible to derive a ranking of the powder's spreadability and to assess the effect of the scrolling velocity of the blade on the quality of the obtained layer surface. In most cases, but remarkably not always, the quality of the spread layer decreases with increasing blade spreading velocity. In agreement with previous studies, the powder flowability ranking estimated with the powder flow factor may strongly disagree with the powder spreadability ranking according to the proposed metrics.

Nomenclature

d_{10}	Particle diameter corresponding to the 10th percentile of the cumulative particle size [m]
$d_{3,2}$	Sauter mean diameter [m]
$d_{4,3}$	Volume mean diameter [m]
d_{50}	Particle diameter corresponding to the 50th percentile of the cumulative particle size [m]
d_{90}	Particle diameter corresponding to the 90th percentile of the cumulative particle size [m]
fc	unconfined yield strength [Pa]
ff	flow factor
h	Height of image [px]
l	Width of image [px]
lr_{60}	Range of lengths including spectral values above 60% of the peak
L	Lower part of the image representing the portion of the powder layer analysed
M	Middle part of the image representing the portion of the powder layer analysed
pl	Peak Lenght [m]
T_m	Melting temperature [°]
U	Upper part of the image representing the portion of the powder layer analysed
X	Spreading direction [m]
Y	Perpendicular direction with respect to the spreading direction in the same spreading plane [m]
Z	Vertical direction [m]

Greek symbols

ρ_b	Bulk density of the powder [kg m^{-3}]
ρ_P	Density of the solid [kg m^{-3}]
σ_1	Major principal stress [Pa]

Acronyms

AM	Additive Manufacturing
AR	Aspect ratio
CT	Collection Tray
CWT	Continuous Wavelet Transform
DEM	Discrete Element Method

DT	Deposition tray
FF	Flow Factor [−]
HR	Hausner Ratio [−]
L	Lower part of the image
M	Middle part of the image
P	Deposition plate
PA6	SINTERLINE® POWDER PA6 3400 HT 110 NATURAL
PA6Black	Ultrasint® PA6 LM BLAK- Low melting Polyamide 6-based powder
PPNAT	Ultrasint® PP nat 01- Polypropylene-based powder [−]
PS	Power spectrum
PSD	Particle Size Distribution
SEM	Scanning Electron Microscopy
SLM	Selective Laser Melting
SLS	Selective Laser Sintering
TPU	Ultrasint TPU ® 88A- Thermoplastic polyurethane
U	Upper part of the image

CRediT authorship contribution statement

Marco Lupo: Investigation, Formal analysis, Visualization, Writing - original draft. **Sina Zinatlou Ajabshir:** Investigation, Software, Formal analysis, Visualization, Writing - original draft. **Daniele Sofia:** Conceptualization, Methodology, Resources, Supervision, Validation. **Diego Barletta:** Conceptualization, Methodology, Validation, Funding acquisition, Writing – review & editing, Supervision. **Massimo Poletto:** Conceptualization, Methodology, Funding acquisition, Supervision, Validation, Writing - review & editing.

Declaration of Competing Interest

The authors declare that they have no known competing financial interests or personal relationships that could have appeared to influence the work reported in this paper.

Data availability

Data will be made available on request.

Acknowledgements

Sina Zinatlou Ajabshir's research grant and part of the research were supported by MATHEGRAM, a Marie SKŁODOWSKA-CURIE Innovative Training Network. MATHEGRAM is funded through the People Programme (Marie SKŁODOWSKA-CURIE Actions) of the European Union's Horizon 2020 Programme H2020 under REA grant agreement No. 813202.

Appendix A. Supplementary data

Supplementary data to this article can be found online at https://doi.org/10.1016/j.powtec.2023.118346.

References

[1] T.D. Ngo, A. Kashani, G. Imbalzano, K.T.Q. Nguyen, D. Hui, Additive manufacturing (3D printing): a review of materials, methods, applications and challenges, Compos. Part B Eng. 143 (2018) 172–196, https://doi.org/10.1016/j.compositesb.2018.02.012.
[2] S.A.M. Tofail, E.P. Koumoulos, A. Bandyopadhyay, S. Bose, L. O'Donoghue, C. Charitidis, Additive manufacturing: scientific and technological challenges, market uptake and opportunities, Mater. Today (2017), https://doi.org/10.1016/j.mattod.2017.07.001.
[3] S. Liu, Y.C. Shin, Additive manufacturing of Ti6Al4V alloy: a review, Mater. Des. (2019), https://doi.org/10.1016/j.matdes.2018.107552.
[4] K.V. Wong, A. Hernandez, A review of additive manufacturing, ISRN Mech. Eng. 2012 (2012) 1–10, https://doi.org/10.5402/2012/208760.
[5] D. Sofia, M. Lupo, D. Barletta, M. Poletto, Validation of an experimental procedure to quantify the effects of powder spreadability on selective laser sintering process, Chem. Eng. Trans. 74 (2019) 397–402, https://doi.org/10.3303/CET1974067.
[6] N.N. Kumbhar, A.V. Mulay, Post processing methods used to improve surface finish of products which are manufactured by additive manufacturing technologies: a review, J. Inst. Eng. Ser. C. (2018), https://doi.org/10.1007/s40032-016-0340-z.
[7] L.I. Escano, N.D. Parab, L. Xiong, Q. Guo, C. Zhao, K. Fezzaa, W. Everhart, T. Sun, L. Chen, Revealing particle-scale powder spreading dynamics in powder-bed-based additive manufacturing process by high-speed x-ray imaging, Sci. Rep. (2018), https://doi.org/10.1038/s41598-018-33376-0.
[8] J. Prescott, R.A. Barnum, On powder flowability, Pharm. Technol. 24 (2000) 60–84.
[9] S. Ziegelmeier, P. Christou, F. Wöllecke, C. Tuck, R. Goodridge, R. Hague, E. Krampe, E. Wintermantel, An experimental study into the effects of bulk and flow behaviour of laser sintering polymer powders on resulting part properties, J. Mater. Process. Technol. 215 (2015) 239–250, https://doi.org/10.1016/J.JMATPROTEC.2014.07.029.
[10] Z. Snow, R. Martukanitz, S. Joshi, On the development of powder spreadability metrics and feedstock requirements for powder bed fusion additive manufacturing, Addit. Manuf. (2019), https://doi.org/10.1016/j.addma.2019.04.017.
[11] M. Ghadiri, M. Pasha, W. Nan, C. Hare, V. Vivacqua, U. Zafar, S. Nezamabadi, A. Lopez, M. Pasha, S. Nadimi, Cohesive powder flow: trends and challenges in characterisation and analysis †, KONA Powder Part. J. (2019) https://doi.org/10.14356/kona.2020018.
[12] H. Chen, Q. Wei, S. Wen, Z. Li, Y. Shi, Flow behavior of powder particles in layering process of selective laser melting: numerical modeling and experimental verification based on discrete element method, Int. J. Mach. Tools Manuf. 123 (2017) 146–159, https://doi.org/10.1016/j.ijmachtools.2017.08.004.
[13] D. Yao, X. An, H. Fu, H. Zhang, X. Yang, Q. Zou, K. Dong, Dynamic investigation on the powder spreading during selective laser melting additive manufacturing, Addit. Manuf. 37 (2021), 101707, https://doi.org/10.1016/j.addma.2020.101707.
[14] M. Schmid, F. Amado, G. Levy, K. Wegener, Flowability of powders for selective laser sintering (SLS) investigated by round robin test, in: High Value Manuf. Proc. 6th Int. Conf. Adv. Res. Virtual Rapid Prototyping, Leir. Port. 1-5 October, 2013, Taylor & Francis, Leiria, Portugal, October 1–5, 2014, pp. 95–99, https://doi.org/10.3929/ETHZ-A-010057806.
[15] D. Ruggi, C. Barrès, J.-Y. Charmeau, R. Fulchiron, D. Barletta, M. Poletto, A quantitative approach to assess high temperature flow properties of a PA 12 powder for laser sintering, Addit. Manuf. 33 (2020), 101143, https://doi.org/10.1016/j.addma.2020.101143.
[16] D. Ruggi, M. Lupo, D. Sofia, C. Barrès, D. Barletta, M. Poletto, Flow properties of polymeric powders for selective laser sintering, Powder Technol. 370 (2020) 288–297, https://doi.org/10.1016/j.powtec.2020.05.069.
[17] I. Tomasetta, D. Barletta, M. Poletto, The high temperature annular shear cell: a modified ring shear tester to measure the flow properties of powders at high temperature, Adv. Powder Technol. 24 (2013) 609–617, https://doi.org/10.1016/j.apt.2012.11.007.
[18] A.B. Spierings, M. Voegtlin, T. Bauer, K. Wegener, Powder flowability characterisation methodology for powder-bed-based metal additive manufacturing, Prog. Addit. Manuf. 1 (2016) 9–20, https://doi.org/10.1007/s40964-015-0001-4.
[19] E. Fereiduni, A. Ghasemi, M. Elbestawi, Characterization of composite powder feedstock from powder bed fusion additive manufacturing perspective, Materials (Basel). 12 (2019) 3673, https://doi.org/10.3390/ma12223673.
[20] S. Xi, P. Zhang, Y. Huang, M. Kong, Q. Yang, G. Li, Laser sintering of cryogenically ground polymer powders into high-performance parts: the role of dry particle coating with a conductive flow agent, Polymer (Guildf). 186 (2020), 122044, https://doi.org/10.1016/j.polymer.2019.122044.
[21] Z. He, C. Ren, A. Zhang, J. Bao, Preparation and properties of styrene ethylene butylene styrene / polypropylene thermoplastic elastomer powder for selective laser sintering 3D printing, J. Appl. Polym. Sci. 138 (2021) 50908, https://doi.org/10.1002/app.50908.
[22] X. Gong, X. Gao, N. Yu, D. Zhang, L. Tan, J. Li, Characterization of thermally treated polypropylene powders with wide sintering window for powder bed fusion of polymers, Polym. Test. 96 (2021), 107078, https://doi.org/10.1016/j.polymertesting.2021.107078.
[23] A. Amado, M. Schmid, G. Levy, K. Wegener, Advances in SLS powder characterization, in: 22nd Annu. Int. Solid Free. Fabr. Symp. - An Addit. Manuf. Conf. SFF 2011, August 8, 2011 - August 10, 2011 12, 2011, pp. 438–452, https://doi.org/10.1088/1751-8113/44/8/085201.
[24] A. Amado, M. Schmid, K. Wegener, Flowability of SLS powders at elevated temperature, in: ETH Zurich, Erfurt, Germany, 2014, https://doi.org/10.3929/ethz-a-010057815.
[25] G. Lumay, F. Boschini, K. Traina, S. Bontempi, J.-C. Remy, R. Cloots, N. Vandewalle, Measuring the flowing properties of powders and grains, Powder Technol. 224 (2012) 19–27, https://doi.org/10.1016/j.powtec.2012.02.015.
[26] G. Yablokova, M. Speirs, J. Van Humbeeck, J.-P. Kruth, J. Schrooten, R. Cloots, F. Boschini, G. Lumay, J. Luyten, Rheological behavior of β-Ti and NiTi powders produced by atomization for SLM production of open porous orthopedic implants, Powder Technol. 283 (2015) 199–209, https://doi.org/10.1016/j.powtec.2015.05.015.
[27] M. Schmid, A. Amado, K. Wegener, Polymer powders for selective laser sintering (SLS), 2015, 160009, https://doi.org/10.1063/1.4918516.
[28] M. Van den Eynde, L. Verbelen, P. Van Puyvelde, Assessing polymer powder flow for the application of laser sintering, Powder Technol. 286 (2015) 151–155, https://doi.org/10.1016/j.powtec.2015.08.004.

[29] M. Ahmed, M. Pasha, W. Nan, M. Ghadiri, A simple method for assessing powder spreadability for additive manufacturing, Powder Technol. (2020), https://doi.org/10.1016/j.powtec.2020.04.033.
[30] H. Salehi, J. Cummins, E. Gallino, N. Harrison, A. Hassanpour, M. Bradley, A new approach to quantify powder's bed surface roughness in additive manufacturing, Powder Technol. 407 (2022), 117614, https://doi.org/10.1016/j.powtec.2022.117614.
[31] M. Mitterlehner, H. Danninger, C. Gierl-Mayer, J. Frank, W. Tomischko, H. Gschiel, Novel testing device and routine to characterise the spreadability of powders for powder bed fusion processes – a problem-oriented approach, Powder Metall. (2022) 1–17, https://doi.org/10.1080/00325899.2021.2023414.
[32] W. Nan, M. Pasha, T. Bonakdar, A. Lopez, U. Zafar, S. Nadimi, M. Ghadiri, Jamming during particle spreading in additive manufacturing, Powder Technol. (2018), https://doi.org/10.1016/j.powtec.2018.07.030.
[33] W. Nan, Y. Gu, Experimental investigation on the spreadability of cohesive and frictional powder, Adv. Powder Technol. 33 (2022), 103466, https://doi.org/10.1016/j.apt.2022.103466.
[34] H. Chen, Y. Chen, Y. Liu, Q. Wei, Y. Shi, W. Yan, Packing quality of powder layer during counter-rolling-type powder spreading process in additive manufacturing, Int. J. Mach. Tools Manuf. 153 (2020), 103553, https://doi.org/10.1016/j.ijmachtools.2020.103553.
[35] L. Cordova, T. Bor, M. de Smit, M. Campos, T. Tinga, Measuring the spreadability of pre-treated and moisturized powders for laser powder bed fusion, Addit. Manuf. 32 (2020), 101082, https://doi.org/10.1016/j.addma.2020.101082.
[36] D. Oropeza, R.W. Penny, D. Gilbert, A.J. Hart, Mechanized spreading of ceramic powder layers for additive manufacturing characterized by transmission x-ray imaging: influence of powder feedstock and spreading parameters on powder layer density, Powder Technol. 117053 (2021), https://doi.org/10.1016/J.POWTEC.2021.117053.
[37] M. Mehrabi, J. Gardy, F.A. Talebi, A. Farshchi, A. Hassanpour, A.E. Bayly, An investigation of the effect of powder flowability on the powder spreading in additive manufacturing, Powder Technol. 413 (2023), 117997, https://doi.org/10.1016/j.powtec.2022.117997.
[38] D. Sofia, Topics towards SLS Process of Ceramic Powders, Doctoral Thesis,, University of Salerno, 2018.
[39] R.D. Goodridge, C.J. Tuck, R.J.M. Hague, Laser sintering of polyamides and other polymers, Prog. Mater. Sci. 57 (2012) 229–267, https://doi.org/10.1016/j.pmatsci.2011.04.001.
[40] W. Nan, M. Ghadiri, Numerical simulation of powder flow during spreading in additive manufacturing, Powder Technol. (2019), https://doi.org/10.1016/j.powtec.2018.10.056.
[41] S. Haeri, Y. Wang, O. Ghita, J. Sun, Discrete element simulation and experimental study of powder spreading process in additive manufacturing, Powder Technol. 306 (2017) 45–54, https://doi.org/10.1016/j.powtec.2016.11.002.
[42] S. Haeri, Optimisation of blade type spreaders for powder bed preparation in additive manufacturing using DEM simulations, Powder Technol. 321 (2017) 94–104, https://doi.org/10.1016/J.POWTEC.2017.08.011.
[43] M. Misiti, Y. Misiti, G. Oppenheim, J.-M. Poggi, Wavelet ToolboxTM 4 User's Guide, 1997.
[44] D. Barletta, M. Poletto, A.C. Santomaso, Chapter 4. Bulk powder flow characterisation techniques, in: C. Hare, A. Hassanpour, M. Pasha (Eds.), Powder Flow, Royal Society of Chemistry, Cambridge, UK, 2019, pp. 64–146, https://doi.org/10.1039/9781788016100-00064.